2024 Scienceline Publication

Journal of Civil Engineering and Urbanism

Volume 14, Issue 3S: 149-157; September 25, 2024 ISSN-2252-0430

DOI: https://dx.doi.org/10.54203/jceu.2024.14

Mapping Buildings from Semi-Informal Settlements Using Non-Parametric Classifiers: A Case of Old Naledi

Wame Mpoeleng, Mooketsi Segobye, Yashon Ouma, Kealeboga Moreri, Bagadzi M. Manisa, Boipuso Nkwae, Lopang Maphale and Nyaladzani Nkhwanana

University of Botswana, Gaborone, Botswana

Corresponding author's Email: segobyem@ub.ac.bw

RESEARCH ARTICLE

PII: S2252043024000014-14

Received: June 25, 2024

Revised: September 02, 2024

Accepted: September 05, 2024

ABSTRACT

Building footprints are essential for planning and designing new infrastructure like water reticulation, electricity transmission, sewer, and road networks. They are also necessary for delivery, census, and disaster management. It is therefore important to have up-to-date maps and GIS databases for service provision. However, mapping building of footprints in semi-informal settlements is problematic because of the spatial heterogeneity of settlements. This study evaluates three non-parametric machine learning algorithms for extracting building footprints from WorldView-2 (WV2) satellite imagery in a semi-informal settlement. WV2 satellite imagery data was fused with gray-level co-occurrence matrices (GLCM) to enhance building extraction. The algorithms used include the Gaussian Mixture Model (GMM), Random Forest (RF), and Support Vector Machine (SVM). The results indicate that GLCM does not improve the detection of buildings when using the GMM algorithm, but it increases building detection with RF and SVM. The GMM algorithm achieved the highest average accuracy of 92% for building detection. However, SVM and RF have an overall accuracy of 79% and 70% respectively. Though RF did not perform very well in identifying individual buildings, its overall accuracy was high. The outcome indicates that machine learning algorithms can adequately map building footprints from high-resolution satellite imagery.

Keywords: Building detection, WorldView-2, machine learning, Gray-Level Co-Occurrence Matrix (GLCM)

INTRODUCTION

Rapid urban development in developing countries has led to the emergence of informal settlements (Hofmann et al.; Mboga et al. 2017; Matarira et al. 2022). UN-Habitat (2015) defines informal settlements as residential areas where (i) there is no security of tenure; (ii) basic services are not available, and (iii) housing is not compliant with current housing and planning regulations. Shortage of basic engineering services, such as water, sewerage and solid waste removal can lead to undesirable living conditions. These services are crucial for attaining the global SDGs, local policies (i.e. Vision 2036), disaster management, and management of humanitarian crises. However, it is difficult to provide basic services because of a shortage of spatial data in informal settlements. Spatial information is required to improve understanding of settlement morphology, population distribution and emerging settlement patterns, which are necessary for decision-making and planning (Mboga et al., 2017). It is therefore critical to have up-to-date maps and GIS databases for better service provision and to identify and quantify services and infrastructure. Conventional, ground surveys and photogrammetry, mapping techniques have been used to gather spatial information. However, they (ground surveys and photogrammetry) are expensive, resource-intensive and time-consuming resulting in data unavailability and information gaps (Mudau and Mhangara, 2021). Consequently, there is a need for methods that can generate reliable and consistent data on the spatial distribution of built-up areas and building structures.

Earth Observation (EO) provides an alternative to conventional mapping. EO allows for the collection of continuous spatial data in satellite images. Technological advances in EO have led to the availability of high-resolution images, which can be leveraged in mapping complex areas like informal settlements. High-resolution imagery has been used in several studies for the extraction of human settlements (Hofmann et al.; Mboga et al., 2017; Shafizadeh-Moghadam et al., 2021), land use and land cover (LULC) (Tassi and Vizzari, 2020; Vizzari, 2022),

and building detection (Zhao et al., 2018; Khatriker and Kumar, 2018). In the building detection studies, Zhao et al. (2018) used convolutional neural networks while (Khatriker and Kumar, 2018) used image segmentation. Accordingly, various methods are used in building footprint extraction, the basic layer in a spatial database.

Feature extraction from remote sensing imagery data can be done through visual image interpretation, traditional pixel-based classification, Object-based image analysis (OBIA) and machine learning techniques (Mudau and Mhangara 2021). Informal settlements are characterised by small buildings, less vegetation, and irregular patterns, hence visual interpretation is labour-intensive and time-consuming. OBIA yields better classification results, however, it requires high computational power and proprietary imaging software (Vizzari, 2022). Machine learning algorithms have also been found to produce good results and are easily available. According to Sheykhmousa et al. (2020), Random Forest (RF), Support Vector Machines (SVM), and deep learning algorithms are the most used classification methods. Deep learning techniques can retrieve complex patterns and informative features from satellite images. However, they are highly dependent on the amount of data. RF and SVM, on the other hand, have been found to learn tasks from a small amount of data, but with competitive results to deep learning (Mboga et al., 2017). GLCM indices are normally used to improve machine learning classification. For example, Burnett et al. (2019) mapped the extent of coconut using a combination of WorldView-2 (WV2) imagery and GLCM textures. While Pantoja et al. (2023) conducted LULC classification using GLCM and Landsat 8 imagery.

This study proposes to use machine-learning classifiers, GMM, RF, and SVM, to map building footprints in Old Naledi, an informal settlement in Gaborone, Botswana, using WV2 satellite imagery. To achieve this the study will (i) investigate the significance of GLCM texture features in detecting building footprints from WV2 images and (ii) explore the performance of machine-learning classifiers in extracting building footprints.

MATERIALS AND METHODS

Study area

Old Naledi, known as "Zola", was chosen as the study area. It is located at the southern tip of Botswana's capital, Gaborone (Figure 1). "Zola" covers a total area of around 159 hectares. The population is 18,050 as of the 2022 census (Statistics Botswana 2022). The origin of Old Naledi can be traced to the construction of Gaborone industrial areas in 1964 (Van Nostrand 1982). The area lacks proper street arrangements and public sanitation facilities. It is comprised of low-income housing which emerged as a semi-informal settlement and is an area with high crime rates in Gaborone. For planning and upgrading the area, the up to date topographical and building footprint is required.

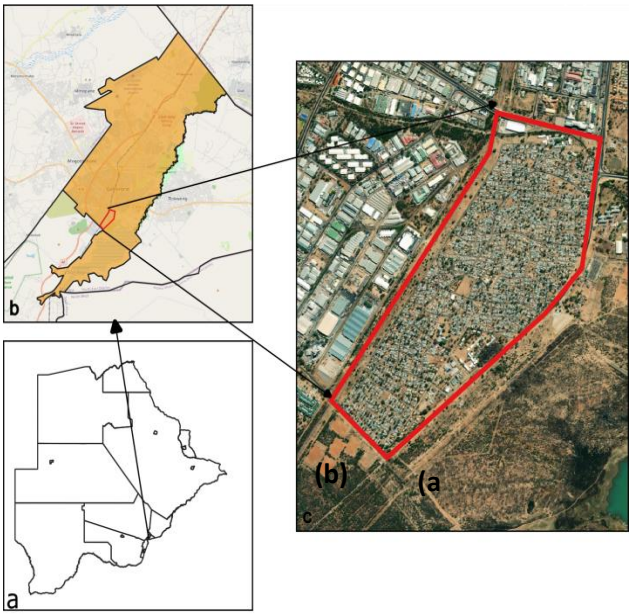

Figure 1. Study area showing (a) Botswana, (b) Gaborone and (c) Old Naledi

Methodology

Figure 2 shows the process used in extracting buildings from high-resolution satellite images. The workflow includes image composition, textural analysis, machine learning (ML) image classification, and accuracy assessment. The first step is to acquire high-resolution images from WV2 and pre-process the image to a multispectral image (MSI). To improve the resolution of the MSI image, pan-sharpening is applied using the panchromatic band of WV2 imagery.

The second stage involves calculating texture metrics using the GLCM technique. The GLCM indices are integrated with the pan-sharpened image input into ML algorithms (GMM, RF, and SVM) to classify the image pixels into buildings, bare soils, trees, roads, and grass. Finally, an accuracy assessment is conducted using the classification metrics outlined in the Accuracy Assessment Section.

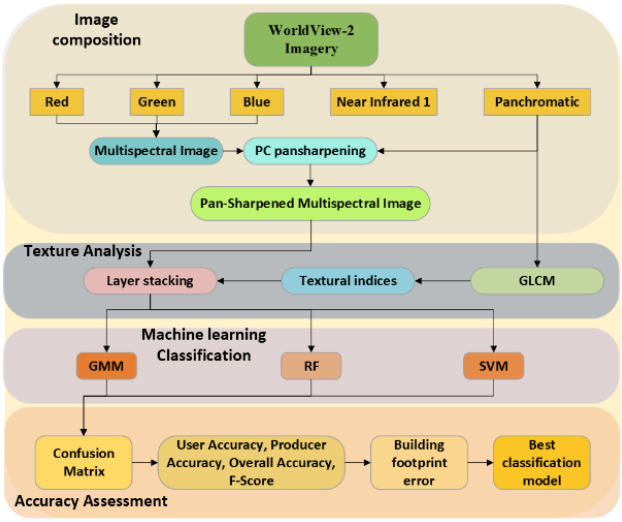

Figure 2. Flowchart of informal settlement classification using machine learning

Table 1. World View-2 spectral bands

Spectral band	Wavelength (nm)	Resolution (m)
Coastal Blue	400 - 450	1.84
Blue	450 - 510	1.84
Green	510 - 580	1.84
Yellow	585 - 625	1.84
Red	630 - 690	1.84
Red Edge	705 - 745	1.84
Near Infrared 1	770 - 895	1.84
Near Infrared 2	860 -1040	1.84
Panchromatic	450 - 800	0.46

Image composition

WorldView-2 (WV2) satellite imagery was used as the primary data source. WV2 is a DigitalGlobe satellite sensor launched in 2009 (Belfiore and Parente 2016). The sensor provides eight spectral bands and a high-resolution panchromatic band (see Table 1). This study utilized the red, green, blue, Near Infrared 1 (NIR1), and panchromatic (PAN) bands of WV2 imagery. A multispectral image (MSI) is created by combining four low-resolution multispectral bands (Red, Green, Blue and Near Infrared 1 (RGBNIR)) through layer stacking (Figure 3(a)). By combining datasets with different signatures, layer stacking can improve the analysis and interpretation of the data and allow the visualisation of complex data.

The RGBNIR MSI image created above is a colour image with a spatial resolution of 1.84 m, and at this resolution, some objects will not be visible. On the other hand, the WV2 Panchromatic band is a monochrome (black and white) image with a spatial resolution of 0.46 m. Thus, the PAN image lacks a realistic true view of the world. The two images can be fused to produce an enhanced image with a high spatial and spectral resolution through a process called pan-sharpening (Li et al. 2017). Pan-sharpening reveals more information than the individual input image, as the image will be rich in spectral content and have high resolution (Fig. 3b).

Gray-level co-occurrence matrix (GLCM) textural features

Textural features are important for classifying data with low inter-class variability (Burnett et al. 2019) as they improve classification and avoid fuzziness (Matarira et al. 2022). The GLCM algorithm is widely used in extracting textural data from remote sensing data (Khatriker and Kumar 2018; Shafizadeh-Moghadam et al. 2021; Matarira et al. 2022). GLCM is used in the computation of spatial dependence of grey levels in an image, it creates a matrix describing the frequency of the appearance of individual pairs of values in a specific image fragment. GLCM textures can be extracted from a single multispectral band, a composite of multispectral bands, or a panchromatic band. The WV2 PAN band was used, because of its high spatial resolution. Seven textural features were extracted from the WV2 PAN, including mean, contrast, variance, second moment, entropy, homogeneity, and dissimilarity. The description of the textures is presented in Table 2.

Figure 3. WorldView-2 satellite images (a) RGBNIR image and (b) pan-sharpened image

Table 2. GLCM features calculated from PAN band and their descriptions

	GLCM Texture	Texture Group	GLCM Texture Description
1	Mean	Statistical	Measures the mean of the gray level sum distribution of the image
2	Contrast	Contrast	Measures the contrast based on the local grey level variation
3	Variance	Statistical	Measures the dispersion of the grey level distribution to emphasize the visual edges of land-cover patches
4	Second Moment	Orderliness	Measures the uniformity or energy of the grey level distribution of the image.
5	Entropy	Orderliness	Measures the degree of the disorder among pixels in the image
6	Homogeneity	Contrast	Measures the smoothness (homogeneity) of the image

Image classification using machine learning

As mentioned, three non-parametric algorithms are applied for the pixel-based image classification, and these are GMM, RF, and SVM. Input data to the machine learning algorithms is the MSI image alone and the seven (7) GLCM textural indices layer-stacked consecutively on the MSI. Therefore, eight (8) input data sets are utilized (Table 3), resulting in 24 classifications.

Table 3. layer-stacked data inputs to ML classification algorithms

Input	Image
1	MSI
2	1 + Mean
3	2 + Variance
4	3 + Contrast
5	4 + Second Moment
6	5 + Homogeneity
7	6 + Entropy
8	7 + Dissimilarity

Gaussian mixture model (GMM)

The GMM model is an unsupervised clustering method that groups subpopulations of a population based on the Gaussian distribution (Wan et al. 2019). The model is composed of multivariate Gaussian components. GMM is then used to distribute data points to the Gaussian components. Equation 1 below represents the GMM model.

$$P(x) = \sum_{i=1}^{k} \pi_i \mathcal{N}(x|\mu_i, \Sigma_i) \ \#(1)$$

were $P(x)$ is the probability of pixel x, K is the number of components in the mixture, π_i is the weight of the i^{th} component, $\mathcal{N}(x|\mu_i, \Sigma_i)$ is the Gaussian distribution, μ_i is the mean vector and Σ_i is the covariance matrix. The matrix weight must satisfy the condition $\sum_{i=1}^{K} \pi_i = 1$ (Menezes and Poojary 2020).

Random forest (RF)

RF is a non-linear, tree-based, supervised machine-learning algorithm that was proposed by Breiman (2001) in 2001. It is an ensemble learning (multiple classifier systems) technique capable of performing both classification and regression analysis (Rahaman et al. 2019). Sub-samples or decision trees are selected through bootstrapping to ensure diversity in the decision trees. The decision trees are then trained through bootstrap aggregation (bagging) to build a model, which guarantees independence among the trees. The models from each decision tree are combined to arrive at the final model. Observations that are not used in a bootstrap sample, which are called "out-of-bag" (OOB), are used for error calculation and variable importance (Cutler et al. 2012).

Support vector machine (SVM)

SVM is a supervised machine learning algorithm for finding the optimal hyperplane that separates a dataset into predefined classes by using training data (Sheykhmousa et al. 2020). In SVM, the goal is to increase the margin of training data closest to the hyperplane from each class (Foody and Mathur 2004). The margin is the distance of training samples closest to the optimal boundary, the samples known as support vectors. The advantages of the SVM are that it is well suited to small complex data and high dimensional spaces.

Accuracy assessment

Classification accuracy assessment was computed from the confusion matrix, which is commonly used in evaluating classified maps (Barsi et al. 2018; Tassi and Vizzari 2020; Vizzari 2022). The matrix shows the number of true positives (TP) for a correct prediction, true negatives (TN) for a correct rejection, false positives (FP) for an incorrect prediction, and false negatives (FN) for a true rejection. The matrix allows for quantitative analysis of the classification using metrics in equations 2 - 5.

$$UA = \frac{TP}{TP + FP} \ \#(2)$$

$$PA = \frac{TP}{TP + FN} \#(3)$$

$$F - Score = 2\frac{UA \times PA}{UA + PA} \ \#(4)$$

$$OA = \frac{TP + TN}{TP + FP + TN + FN} \#(5)$$

where PA is the producer's accuracy, UA is the user accuracy mearing the, OA is the overall accuracy. PA gives the ratio of the true detected pixels against the building pixels and is related to omission error ($1 - PA$). UA is the ratio of detected pixels against all detected pixels and is concerned with the commission error ($1 - UA$). The F-score is a more sensitive and specific measure of the reliability of a classifier as it combines PA and UA.

RESULTS AND DISCUSSION

Significance of GLCM textures

Figure 4 shows an extract from the classification for each input and classification model. The figure shows more detail for input 1 (MSI) and less for inputs 2 – 8, which were layer-stacked with GLCM textures, in the GMM classification. This could indicate that GLCM textures cause GMM to overfit or underfit the data. For the RF algorithm, all images are similar showing that GLCM textures have less influence on building extraction. The SVM classification shows more detail when GLCM textures are layer-stacked on the RGBNIR image. Thus, GLCM textures improve SVM classification.

Table 4 shows the quantitative classification analysis for each input data and classification model. Table 4 confirms the results in Figure 4 results, from which it is evident that GLCM texture reduces the predicting power of GMM. When textures are introduced, the sensitivity of prediction is reduced as shown by the low PA values. The variation of PA and UA values is small for the RF classification, hence GLCM textures have less impact on RF building detection. SVM classification shows fewer false hits for input 3 (MSI + MEAN + CONTRAST) with a PA value of 99.28%. Contrast, entropy and dissimilarity reduce the predicting power of SVM.

The F-score and OA (Table 4 and Figure 5) show that the input with the best precision, sensitivity, and accuracy was input 1 for GMM and input 3 for SVM. Therefore, inputs 1 and 3 are selected as the representatives of the GMM and SVM models respectively.

For RF the inputs with the highest values differ, input 7 has the highest F-score value whereas input 6 has the highest OA value (Table 4 and Figure 5). As OA is the accuracy of a classifier for all classes, input 6 is selected as the representative for the RF model. According to Figure 6, RF is more consistent in identifying the different classes and is more appropriate for the classification in this area.

Table 4. Classification results of the different models

Input	GMM			RF			SVM		
	PA (%)	UA (%)	F-score (%)	PA (%)	UA (%)	F-score (%)	PA (%)	VA (%)	F-score (%)
1	99.3	99.47	99.38	99.51	99.51	99.51	99.12	98.48	98.80
2	97.77	99.35	98.55	99.04	99.61	99.32	98.64	99.53	99.08
3	97.51	99.00	98.25	99.26	99.76	99.51	99.28	99.36	99.32
4	97.18	98.74	97.95	99.57	99.82	99.69	98.08	99.55	98.81
5	94.23	89.51	91.81	99.49	99.90	99.69	99.20	98.97	99.08
6	93.65	89.30	91.42	99.59	99.92	99.75	98.88	99.28	99.08
7	93.65	89.30	91.42	99.79	99.96	99.87	98.93	99.01	98.97
8	93.44	89.26	91.30	99.45	99.69	99.57	98.89	98.89	98.89

Figure 4. Classification results from the three models (GMM, RF, and SVM). The numbers on the left indicate the layer-stacked datasets derived from Table 3

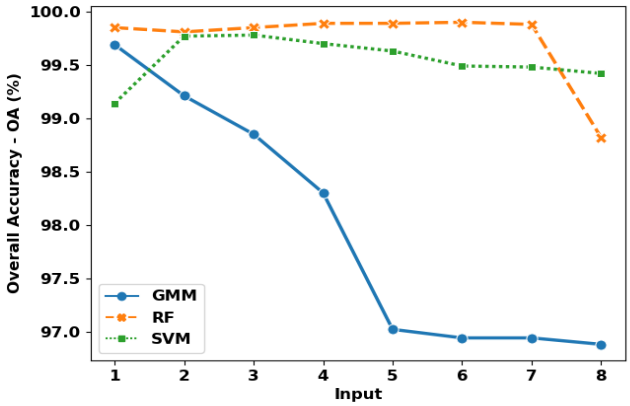

Figure 5. Overall accuracy of the classification. Input 1 is the WV2 RGBNIR image. Inputs 2 - 8 contain input 1 layer-stacked with textural features

Validation of building extraction

Three different portions were selected from the reference raster figure and compared with the best classification results from each model. The selected

portions had a high ratio of buildings. For GMM the best classification used MSI as input, whereas for RF the best classification was input 6, which has MSI + Textures (Mean, Variance, Contrast, Second Moment, and homogeneity). Input 3, which had MSI + Textures (Mean, Variance, Contrast) gave the best classification for the SVM algorithm; hence it was used here. Pixel differences were calculated between the two raster layers, reference and classified image, to find the error of building detection from each algorithm. Consequently, giving the accuracy of each model.

Figures 6–8 show the prediction errors from each algorithm and portion. A visual inspection of the images indicates that GMM gave superior results, followed by SVM and RF. RF shows misclassifications especially at the boundaries even though the input image had GLCM textural indices. In terms of building edge detection GMM and SVM gave good results. On the other hand, RF was not able to identify the building edges especially on portion 2 and 3.

Quantitative analysis indicates that GMM had fewer prediction errors with an average accuracy of 92.38% for all the portions. The highest accuracy of GMM was in portion 3 at 99.8%. RF and SVM had average accuracies of 70.53% and 79.26% respectively. Portion 1 results were the most accurate, with the lowest accuracy of 86.5% for SVM (Figure 6). Portion 2 (Figure 7), which had a high density of buildings, had the lowest accuracy for all the models at 82.90%, 64.78%, and 54.5% for GMM, SVM, and RF respectively.

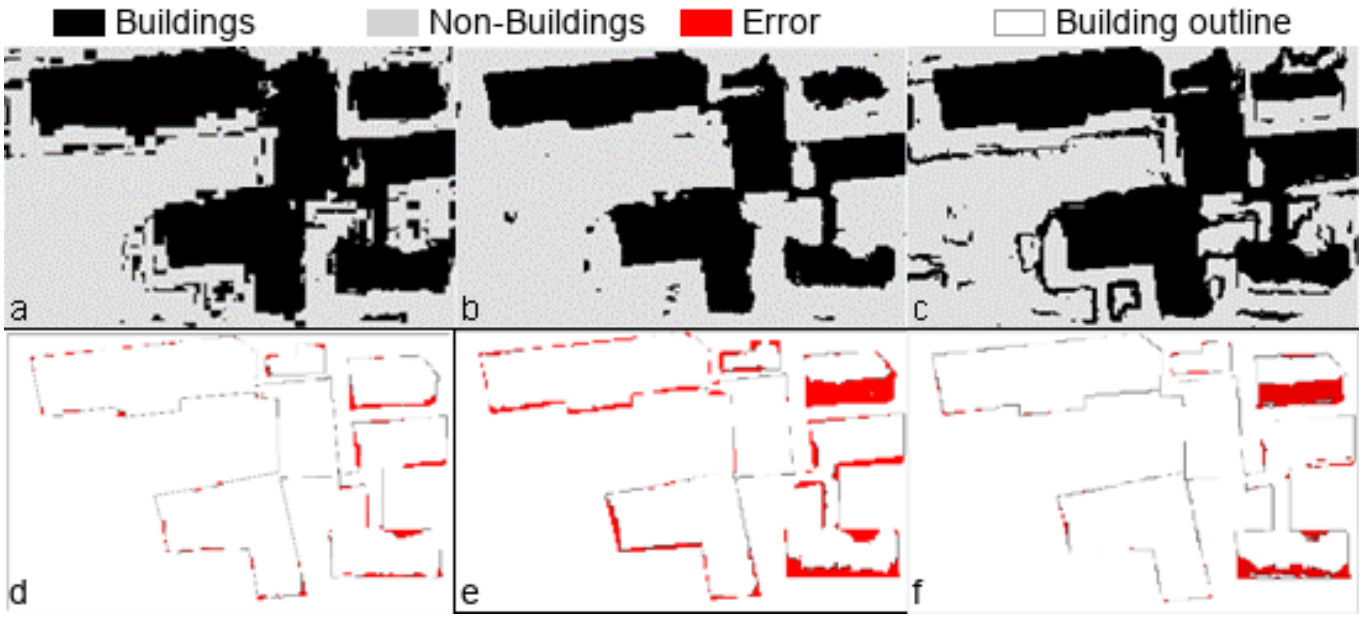

Figure 6. Classification results for image portion 1. (a), (b), and (c) are classification results for GMM, RF, and SVM respectively. Errors of the models are (d) GMM, (e) RF, and (f) SVM

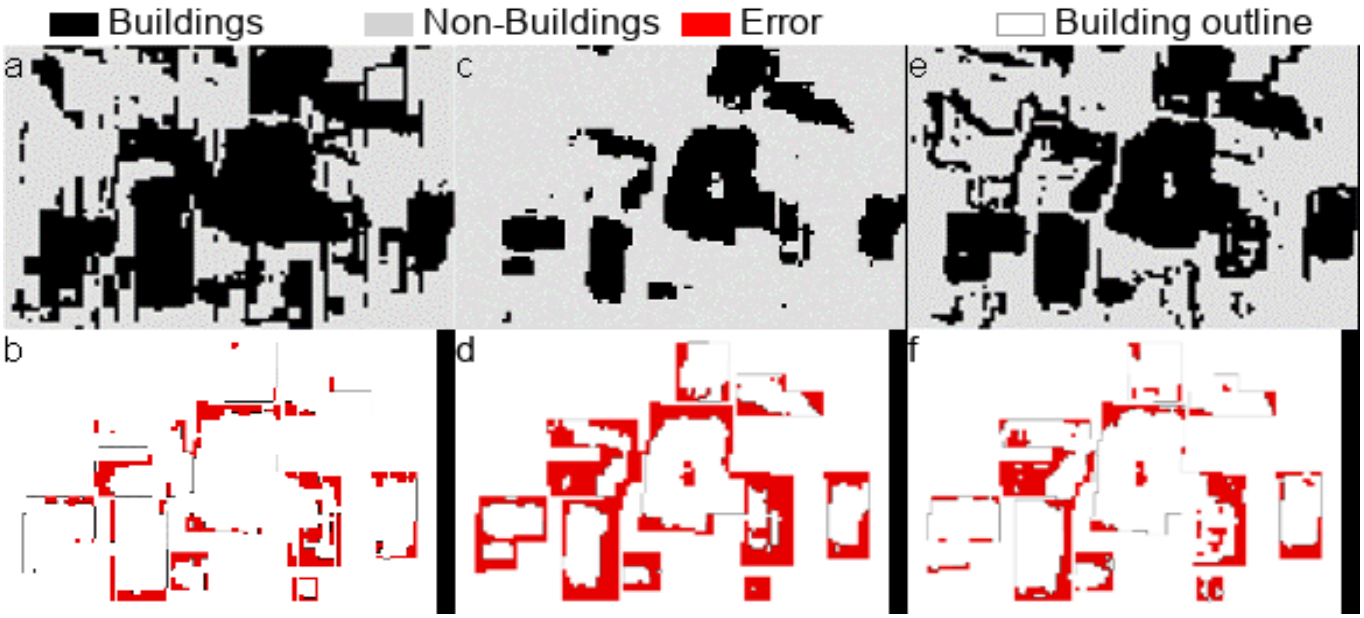

Figure 7. Classification results for image portion 2. (a), (c), and (e) are classification results for GMM, RF, and SVM respectively. Errors of the models are (b) GMM, (d) RF, and (f) SVM.

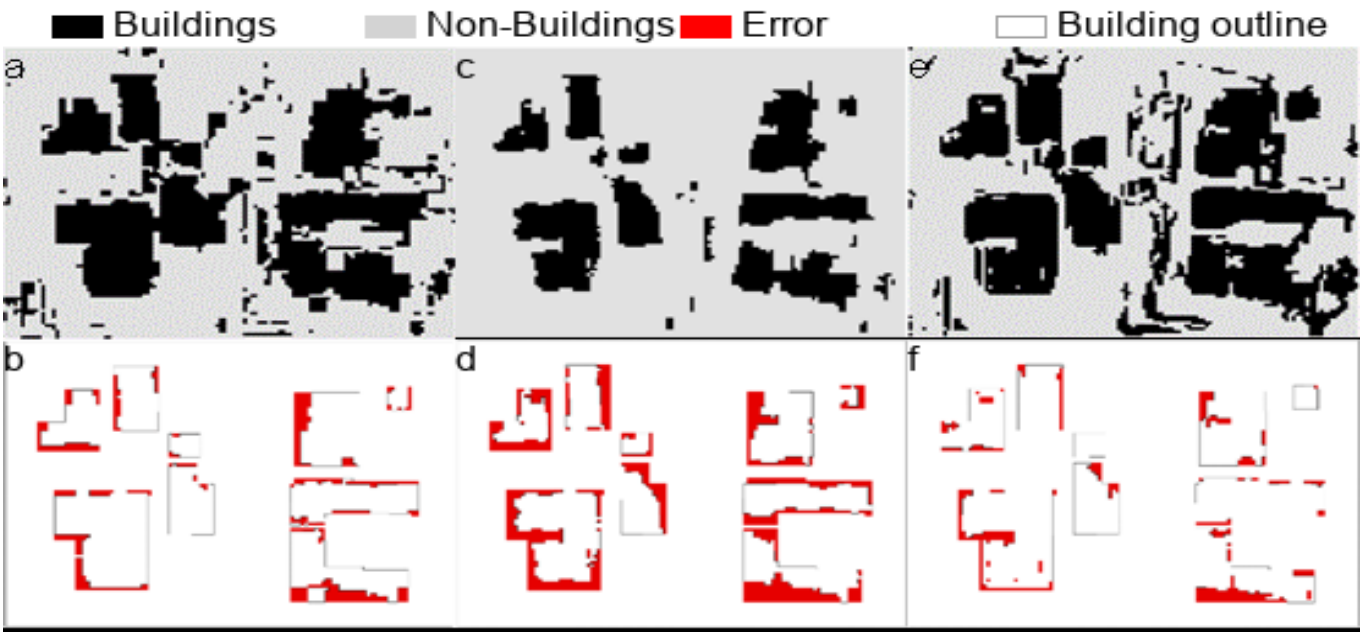

Figure 8. Classification results for portion 3. (a), (c), and (e) are classification results for GMM, RF, and SVM respectively. Errors of the models are (b) GMM, (d) RF, and (f) SVM.

CONCLUSIONS

The study has shown that integrating remote sensing and machine learning can adequately map informal settlements. The current results demonstrate that GMM performs poorly with textural indices, whereas RF and SVM need textural indices to classify features on an image. The highest OA for RF and SVM of 99.90% and 99.78% respectively, were obtained when textural indices were fused into the WV-2 image. RF performed exceptionally well in detecting different classes in the image. However, RF did not perform well in extracting building footprints with an average accuracy of 70.5%. The model that performed well in detecting building

footprints was GMM with an accuracy of 92.4%. The outcome of settlement maps from this study was satisfactory, hence remote sensing and machine learning could be used in mapping traditional villages as they have the same spatial structure as informal settlements.

DECLARATIONS

Corresponding Author

Correspondence and requests for materials should be addressed to; E-mail: segobyem@ub.ac.bw; ORCID: https://orcid.org/0009-0008-4028-1763

Data availability

The datasets used and/or analysed during the current study are available from the corresponding author on reasonable request.

Acknowledgements

The authors would like to acknowledge the University of Botswana for creating a conducive environment to conducting this research.

Authors' contribution

WM performed the experiments and analysed the data obtained. MS and WM wrote the manuscript and designed the figures in consultation with YO. YO conceived and supervised the study. KM, BM, LM, BN, and NN assisted in the management of the research project. All Authors read and approve the content of the final manuscript.

Competing interests

The authors declare no competing interests in this research and publication.

REFERENCES

Barsi Á, Kugler Zs, László I, et al (2018). Accuracy Dimensions in Remote Sensing. The International Archives of the Photogrammetry, Remote Sensing and Spatial Information Sciences XLII–3:61–67. DOI: https://doi.org/10.5194/isprs-archives-XLII-3-61-2018; Google Scholar

Belfiore O, Parente C (2016). Comparison of Different Algorithms to Orthorectify WorldView-2 Satellite Imagery. Algorithms 9:67. DOI: https://doi.org/10.3390/a9040067; Google Scholar

Breiman L (2001). Random Forests. Mach Learn 45:5–32. https://doi.org/10.1023/A:1010933404324

Burnett MW, White TD, McCauley DJ, et al (2019). Quantifying coconut palm extent on Pacific islands using spectral and textural analysis of very high-resolution imagery. Int J Remote Sens 40:7329–7355. DOI: https://doi.org/10.1080/01431161.2019.1594440; Google Scholar

Cutler A, Cutler RD, Stevens JR (2012). Random Forest. In: Zhang C, Ma Y (eds). Ensemble Machine Learning: Methods and Applications. Springer US, Boston, MA, pp 157–176. Google Scholar

Foody GM, Mathur A (2004). A relative evaluation of multiclass image classification by support vector machines. IEEE Transactions on Geoscience and Remote Sensing 42:1335–1343. DOI: https://doi.org/10.1109/TGRS.2004.827257; Google Scholar

Hofmann P, Strobl J, Blaschke T, Kux H (2008). Detecting informal settlements from QuickBird data in Rio de Janeiro using an object based approach. In: Object-Based Image Analysis. Springer Berlin Heidelberg, Berlin, Heidelberg, pp 531–553. Google Scholar

Khatriker S, Kumar M (2018). Building Footprint Extraction from High Resolution Satellite Imagery Using Segmentation. The International Archives of the Photogrammetry, Remote Sensing and Spatial Information Sciences XLII–5:123–128. DOI: https://doi.org/10.5194/isprs-archives-XLII-5-123-2018; Google Scholar

Li S, Kang X, Fang L, et al (2017). Pixel-level image fusion: A survey of the state of the art. Information Fusion 33:100–112. DOI: https://doi.org/10.1016/j.inffus.2016.05.004; Google Scholar

Matarira D, Mutanga O, Naidu M, Vizzari M (2022). Object-Based Informal Settlement Mapping in Google Earth Engine Using the Integration of Sentinel-1, Sentinel-2, and PlanetScope Satellite Data. Land (Basel) 12:99. DOI: https://doi.org/10.3390/land12010099; Google Scholar

Mboga N, Persello C, Bergado J, Stein A (2017). Detection of Informal Settlements from VHR Images Using Convolutional Neural Networks. Remote Sens (Basel) 9:1106. DOI https://doi.org/10.3390/rs9111106; Google Scholar

Menezes J, Poojary N (2020). A fusion approach to classify hyperspectral oil spill data. Multimed Tools Appl 79:5399–5418. https://doi.org/10.1007/s11042-018-6709-7; Google Scholar

Mudau N, Mhangara P (2021) Investigation of Informal Settlement Indicators in a Densely Populated Area Using Very High Spatial Resolution Satellite Imagery. Sustainability 13:4735. DOI https://doi.org/10.3390/su13094735; Google Scholar

Pantoja DA, Spenassato D, Emmendorfer LR (2023) Comparison Between Classification Algorithms: Gaussian Mixture Model - GMM and Random Forest - RF, for Landsat 8 Images. Revista de Gestão Social e Ambiental 16:e03234. DOI https://doi.org/10.24857/rgsa.v16n3-015; Google Scholar

Rahaman MM, Thakur B, Kalra A, et al (2019) Estimating high-resolution groundwater storage from GRACE: A random forest approach. Environments - MDPI 6:. DOI https://doi.org/10.3390/environments6060063; Google Scholar

Shafizadeh-Moghadam H, Khazaei M, Alavipanah SK, Weng Q (2021). Google Earth Engine for large-scale land use and land cover mapping: an object-based classification approach using spectral, textural and topographical factors. GIsci

Remote Sens 58:914–928. DOI: https://doi.org/10.1080/15481603.2021.1947623; Google Scholar

Sheykhmousa M, Mahdianpari M, Ghanbari H, et al (2020). Support Vector Machine Versus Random Forest for Remote Sensing Image Classification: A Meta-Analysis and Systematic Review. IEEE J Sel Top Appl Earth Obs Remote Sens 13:6308–6325. DOI: https://doi.org/10.1109/JSTARS.2020.3026724; Google Scholar

Statistics Botswana (2022). Population and Housing Census 2022 Population of Cities, Towns and Villages Version 2. https://dataspace.princeton.edu/handle/88435/dsp01ms35tc881; Google Scholar

Tassi A, Vizzari M (2020). Object-Oriented LULC Classification in Google Earth Engine Combining SNIC, GLCM, and Machine Learning Algorithms. Remote Sens (Basel) 12:3776. DOI: https://doi.org/10.3390/rs12223776; Google Scholar

UN-Habitat (2015). Habitat III issue paper 22 - informal settlements. DOI: https://habitat3.org/wp-content/uploads/Habitat-III-Issue-Paper-22_Informal-Settlements-2.0.pdf. Accessed 9 Jun 2024

Van Nostrand J (1982). Old Naledi: The Village Becomes a Town: An Outline of the Old Naledi Squatter Upgrading Project, Gaborone, Botswana. James lorimer & Company, Toronto

Vizzari M (2022). PlanetScope, Sentinel-2, and Sentinel-1 Data Integration for Object-Based Land Cover Classification in Google Earth Engine. Remote Sens (Basel) 14:2628. DOI: https://doi.org/10.3390/rs14112628; Google Scholar

Wan H, Wang H, Scotney B, Liu J (2019) A Novel Gaussian Mixture Model for Classification. In: 2019 IEEE International Conference on Systems, Man and Cybernetics (SMC). IEEE, pp 3298–3303. DOI: https://doi.org/10.1109/SMC.2019.8914215; Google Scholar

Zhao K, Kang J, Jung J, Sohn G (2018). Building Extraction from Satellite Images Using Mask R-CNN with Building Boundary Regularization. In: 2018 IEEE/CVF Conference on Computer Vision and Pattern Recognition Workshops (CVPRW). IEEE, pp 242–2424. Google Scholar; https://openaccess.thecvf.com/content_cvpr_2018_workshops/w4/html/Zhao_Building_Extraction_From_CVPR_2018_paper.html